# Climate Change mitigation effects: How do potential $CO_2$ leaks from a sub-seabed storage site in the Norwegian Sea affect *Astarte* sp. bivalves?

Estefanía Bonnail [1*], Ana R. Borrero-Santiago [2], Trond Nordtug [3], Ida Beathe Øverjordet [3], Daniel Franklin Krause [3], Murat V. Ardelan [2]

[1] Centro de Investigaciones Costeras-Universidad de Atacama (CIC-UDA). University of Atacama, Copiapó, Chile.

[2] Department of Chemistry, Norwegian Science and Technology University (NTNU), Trondheim, Norway.

[3] SINTEF Ocean, Environment and New Resources, Trondheim, Norway.

*corresponding author: estefania.bonnail@uda.cl

## Abstract

Carbon capture and storage (CCS) is one of the most promising mitigation strategies for reducing the emissions of carbon dioxide ($CO_2$) to the atmosphere and may substantially help to decelerate global warming. There is an increasing demand for CCS sites. Nevertheless, there is a lack of knowledge of the environmental risk associated with potential leakage of $CO_2$ from the storage sites; and even more, what happens when the seepage stops. Can the environment return to the initial equilibrium? Potential effects on native macrofauna were studied under a scenario of a 50-day $CO_2$ leakage, and the subsequent leak closure. To accomplish the objective, Trondheim Fjord sediments and clams were exposed to an acidified environment (pH 6.9) at 29 atm for 5 weeks followed by a 14-day recovery at normal seawater conditions (pH 8.0, 29 atm).

Growth and survival of clams exposed to pressure (29 atm) and reduced pH (6.9) did not significantly differ from control clams kept at 1 atm in natural seawater. Furthermore, bioaccumulation of elements in the soft tissue of clams did not register significant variations for most of the analysed elements (Cd, Cr, Pb, and Ti), while other elements (As, Cu, Fe, Ni) had decreasing concentrations in tissues under acidified conditions in contrast to Na and Mg, which registered an uptake (*Ku*) of 111 and 9.92 µg $g^{-1}$dw $d^{-1}$, respectively. This *Ku* may be altered due to the stress induced by acidification; and the element concentration being released from sediments was not highly affected at that pH. Therefore, a 1 unit drop in pH at the seafloor for several weeks does not appear to pose a risk for the clams.

**Keywords:** Carbon Capture Storage risks; *Astarte* sp.; $CO_2$ impacts; metal bioaccumulation; shell growth rate.

## 1. Introduction

Carbon dioxide ($CO_2$) sequestration and injection into deep geological formations is considered a mitigation option for reducing global warming (IPCC, 2013). This method, known as carbon capture and storage (CCS), is one of the most promising mitigation strategies for reducing the climate effects of $CO_2$ emissions to the atmosphere (Leung et al., 2014). Therefore, pumping large amounts of $CO_2$ into deep saline aquifers are currently being investigated as an environmentally acceptable $CO_2$ disposal method (Bachu and Adams, 2003). According to the CCS Market Size and Forecast Report 2014-2025 (MRR, 2016), there is an increasing demand for CCS in Europe, and the Asia Pacific CCS market expected to rise at 16.4% annually until 2024; meanwhile, the USA accounts for 75% of the global carbon capture (30 million tons per annum) for enhanced oil recovery operations as a clean technology (Market Reports World, 2019). It is estimated that $CO_2$-

enhanced oil recovery might lead to the storage of 10-100 Mt $CO_2$ per year (NPD, 2010). The project "One North Sea" evaluated the feasibility of the North Sea to host future CCS activities. The Norwegian Petroleum Directorate (NPD) has worked for some years on the mapping of offshore $CO_2$ storage sites related to specific CCS projects (NPD, 2010). According to the NDP, the most suited geological formations for the $CO_2$ storage are located in the Norwegian Shelf. Hence, in Norway, there are several reservoirs with the appropriate characteristics to store large amounts of $CO_2$ (Riis and Halland, 2014). The Global CCS Institute highlighted the need of establishing (region-specific) public/private business models that better manage risk allocation between the capture, transport, and storage elements of the CCS chain to reduce overall risks (Global CCS Institute, 2017). The risk assessment of CCS is still incomplete for many regions due to the lack of relevant data for different geological scenarios and surrounding ecosystems. Therefore, taking into account that potential leakages from CCS can promote acidification of water and sediment (Dewar et al., 2013), and mobilization of metals from sub-seabed geological formations (Ardelan et al., 2009; De Orte et al., 2014, 2018; Rodriguez-Romero et al., 2014a; Borrero et al., 2017), specimens of the genus *Astarte* sp. were used as target species in order to test potential risks associated with bivalve macrobenthic infauna in the Norwegian Shelf. Potential effects of $CO_2$ leakages on the benthic ecosystem have mainly been studied at 1 atm, both biological effects (e.g. Bautista-Chamizo et al., 2016; Borrero-Santiago et al., 2016, 2017; Basallote et al., 2018; Świeżak et al., 2018; Sokołowski et al., 2018; Conradi et al., 2019) and changes in seawater chemistry (Payán et al., 2012; Lichtschlag et al., 2015; De Orte et al., 2018). Several studies have mimicked realistic conditions addressing pressure as a variable (Ardelan et al., 2012; Molari et al., 2018, 2019; Basallote et al., 2020), but further studies are needed to evaluate the effects of the compressibility of $CO_2$ (Vilarrasa et al., 2009). The current study appears to be the first research project evaluating recovery of the environment and clams after acidification (pH 6,9) at high pressure (29 atm).

*Astarte* is a complex and cosmopolitan genus marine bivalve, with numerous species described within a circumpolar panarctic distribution (Zetter, 2001- *A. borealis*; Olsen et al., 2009- *A. sulcata*). It resists brackish environments, as the Baltic Sea. It is also resistant to anoxia (Theede et al., 1969; Abele-Oeschger and Oeschger, 1995) and pollution, therefore, it has previously used for monitoring (Olsen et al., 2009).

We studied the possible effects that might affect sub-seabed macrobenthic fauna in a realistic test emulating a potential $CO_2$ leakage (50 days) from a CCS reservoir in the North Sea. The experiment involved exposing sediments containing bivalves (using *Astarte* sp. as the target species) to seawater acidification (down to a pH of 7) within a high-pressure tank. The biological responses were also assessed 14 days after $CO_2$ leakage cessation. Clam mortality, growth, and bioaccumulation of trace elements in soft tissue were assessed to support environmental risk assessment of sub-seabed CCS implementation.

## 2. Materials and Methods

### 2.1.Sampling survey

Sediment was collected using a box corer and subsequently transferred into different plastic containers. Individuals of the bivalve *Astarte* sp. were collected by benthic sledge (Sneli, 1998) dredged between Vikhammer and Malvik (160-180 m depth) in the Trondheim Fjord (Figure 1). Before the experiments, clams were placed in chambers for 72 hours with a continuous flow of filter water from the Trondheim Fjord for gut depuration.

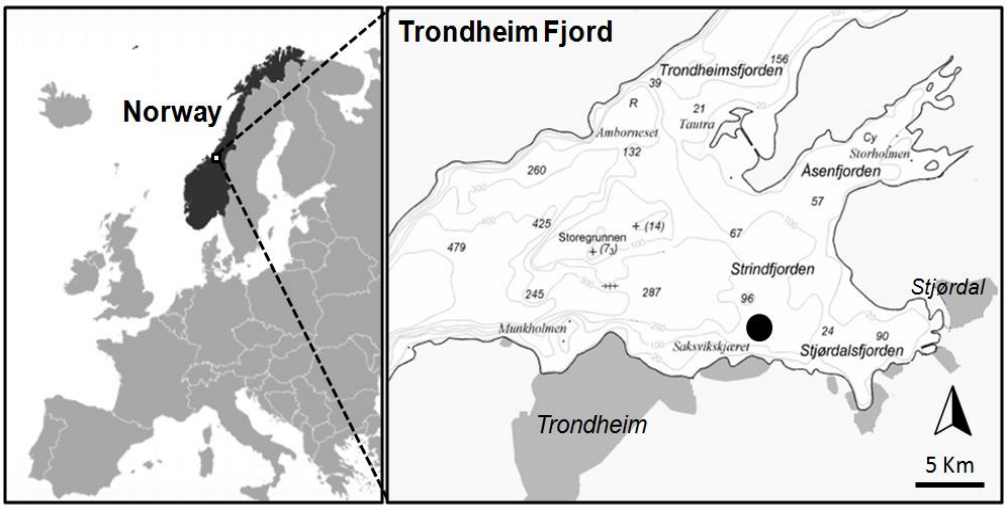


**Figure 1.** Map of Trondheim Fjord location (Norway, left) and bathymetry (m depth, right). The black circle indicates the sediment and clam sampling location in the Trondheim Fjord (Modified from the Geological Survey of Norway, Marine maps, 2017).

## 2.2.Experimental set up: The titanium high-pressure TiTank™

The Karl-Erik TiTank (Figure 2a) was developed to evaluate the direct and secondary effects of potential leakage from sub-seabed $CO_2$ storage sites on seawater geochemistry and biology. It consists of a high pressure (max 30 atm) titanium tank suitable to perform small-scale mesocosm experiments (Ardelan et al., 2012). The tank has an internal rotating carousel that can hold up to 54 trays with samples. Each row of the carousel can host three trays that can be individually sampled.

The tank is equipped with an external decompression sluice so that samples, in this case individual trays, can be collected without affecting the pressure of the main water body of the tank (Figure 2a). The selection of samples is administered with internal cameras and rotation of the carousel along with a motorized slide mechanism that pushes the samples into the decompression sluice.

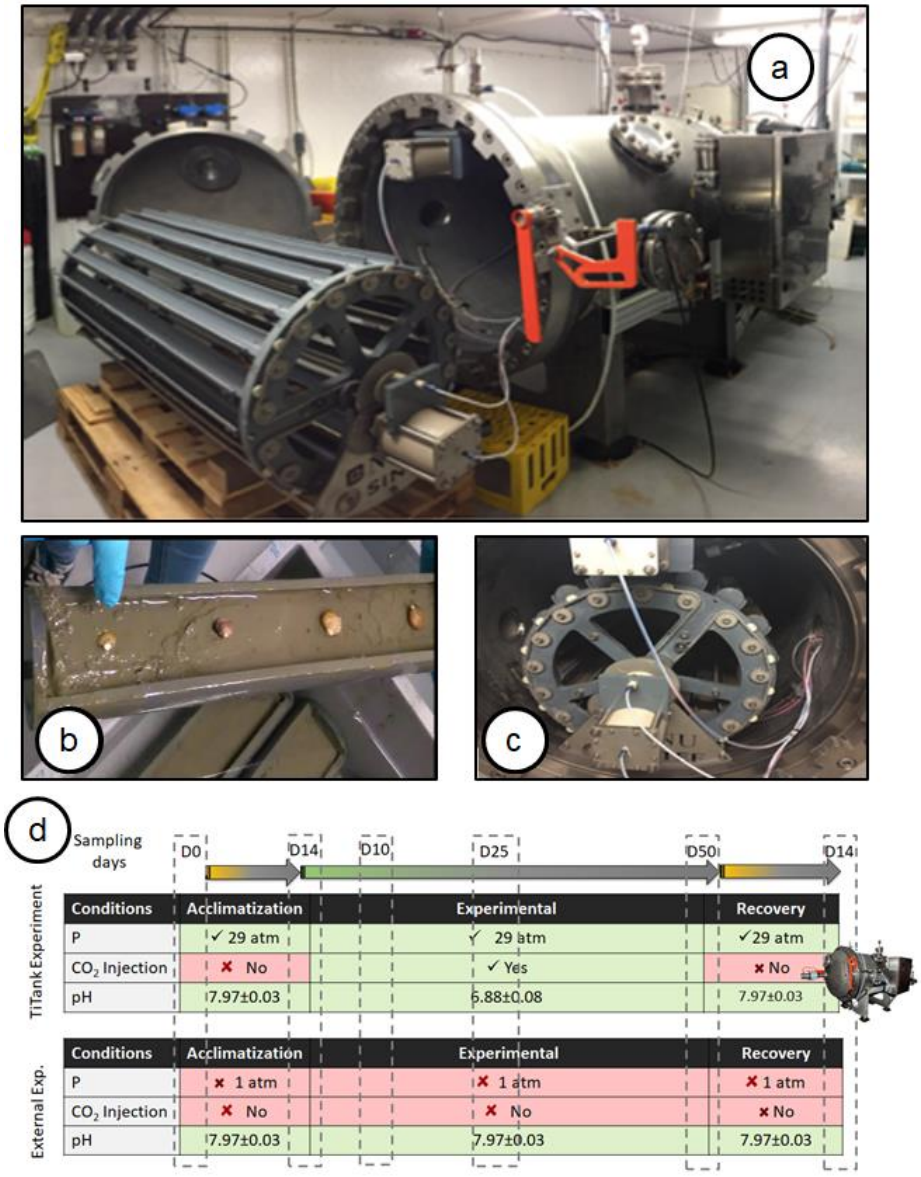


**Figure 2**. Pictures of the titanium tank (TiTank) setup. a) The TiTank and the carousel without the trays. b) Trays with sediment from Trondheim Fjord and *Astarte* sp. c) Carousel with trays inside the TiTank. d) Experimental set up (experiment in the TiTank and external experiment: pressure (P), $CO_2$ injection, and pH reached) and sampling collection schedule ($n$ = 24/ day, discontinuous lines, Dx = number of days from the start).

Homogenized sediments and four clams were placed in each of the trays (Figure 2b). Once the TiTank was closed, filtered seawater from the Trondheim Fjord flowed continuously (0.5 L $min^{-1}$)

through the tank. The pressure was regulated at 29 atm to simulate a depth of 290 m, which corresponds to portions of the Norwegian Continental Shelf seabed. Scientific 5.2 pure $CO_2$ (HiQ, AGA) was dosed into the tank through a mass flow controller via a constant dosing set point to obtain a simulated $CO_2$ leakage resulting in a pH of approximately 7.0. The pH was measured during the experiment using a Mettler Toledo combination pH/redox sensor (Mettler Toledo, PT4805-DXK-S8/120; Urdorf Switzerland) coupled with a thermometer (Mettler Toledo M300 Urdorf, Switzerland). A Thermo Scientific Orion 5-star multifunction meter coupled with a conductivity sensor (Thermo Scientific, Oslo, Norway) measured the salinity. Both meters also included temperature probes. The dissolved oxygen was measured with a (Hach LDO-HQ20 Portable Oxygen Meter; Düsseldorf, Germany) sensor coupled in the inner Titank.

*2.2.1. Bioassay set up*

Three scenarios were selected to assess the potential effects of leakage (Figure 2d) at high pressure (29 atm) into the TiTank with sediments from Trondheim Fjord (pH 7.97 ± 0.03) at 8.3°C with continuous renewable water from Trondheim Fjord (Figure 2d): (i) acclimatization period (no $CO_2$ injection for 14 days); (ii) simulation of leakage as exposure ($CO_2$ injection for 50 days); and (iii) simulation of leak cessation as a recovery period (no $CO_2$ injection for 14 days). An external experiment was also set up at 1 atm with no injection of $CO_2$ in parallel with the TiTank experiment.

Clams ($n$ =132 as $n_{\text{TiTank}}$ = 60; $n_{\text{external}}$ = 60; $n_{\text{background}}$ = 12) were divided into four different size groups (L: 220 ± 12 mm, M: 195 ± 9 mm, S: 168 ± 12 mm, and XS: 119±18 mm) and systematically distributed in the trays. A group of clams was initially reserved for analysis of background element concentration in the soft tissue. During the experiment, clams were continuously fed with a mixture of microalgae of *Rhodomonas baltica*, *Dunaliella tertiolecta*,

138 *Tioschrysis lutea* (0.26: 0.17: 0.29 mg $L^{-1}$ algal wet weight) to avoid food limitation. Dark
139 conditions, temperature (8°C), and dissolved oxygen concentrations at or higher than 94% were
140 maintained during the entire experiment.
141 Every sampling day (Figure 2d), twelve clams from Titank and twelve from external experiment
142 were collected and remained for 24 h in clean water from the TiTank outlet effluent for gut
143 depuration. Mortality, shell width and length, and whole weight measurements were recorded.
144
145 2.3. Analytical procedures
146 *2.3.1. Calcein staining and shell growth measurements*
147 Prior to the TiTank experiment, the external shell surfaces of the organisms were carefully cleaned
148 with a brush to remove organic particles and/or residues before staining with calcein fluorochrome.
149 The chemical marking was carried out by immersion in a solution of 250 mg $L^{-1}$ of calcein (CAS-
150 No: 1461-15-0) in Trondheim Fjord water in dark conditions for 24 h . Shells were wiped dry with a
151 towel and both sides photographed with Nikon Digital Sight DS-Fi1 coupled with a luminescence
152 microscope Leica MGD41 excited at $\lambda$ = 460-490 nm to assess shell health.

153 A total of 130 clams were sampled for determining shell growth according to Linard et al. (2011).
154 Post sampling, individual shells were embedded in the cold-settling resin Epoxy™ before
155 transverse slicing and polishing. Slides were examined under a fluorescence microscope and high-
156 resolution images were collected from the peripheral rim of the shell (Figure 2A). Shell growth was
157 estimated as the maximum thickness of the deposited shell between the fluorescent calcein marking
158 and the inner shell surface at the peripheral rim of the shell (Figure 2B; Sokołowski et al., 2018).
159 Measurements were performed on collected images by ImageJ® software by measuring the width
160 of the growth zone in pixels and converting to µm based on microscope images of calibrated scales
161 at corresponding magnifications. The same procedure was used for determining shell length.

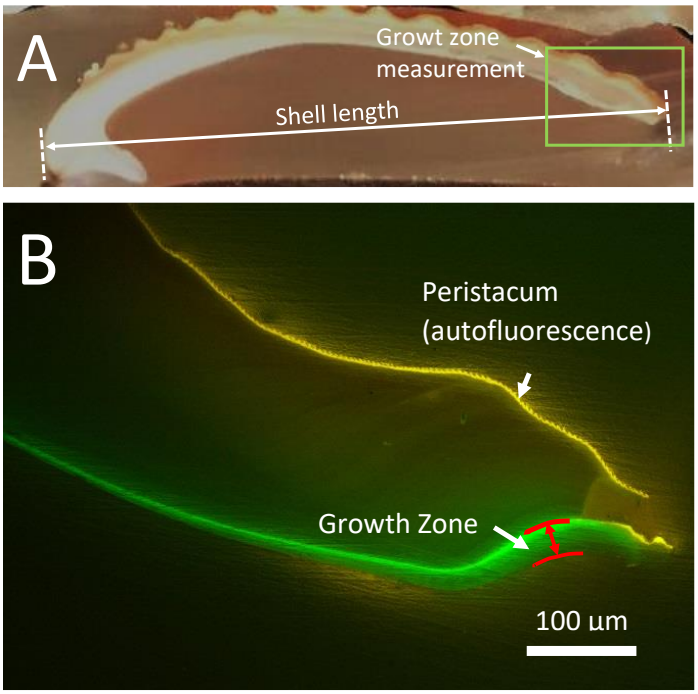


**Figure 3**. Growth measurements with Calcein staining A; Shell cross-section in *Astarte* sp. with indication of the section selected for analysis of shell growth. B: Fluorescence image of the peripheral section of the shell. The maximum thickness of the growth zone (indicated by red lines) was measured as the largest distance between the Calcein fluorochrome marks in green colour and the inner surface of the shell.

*2.3.2. Carbonate system speciation*

**C**arbonate system speciation in seawater (outflow) such as bicarbonate ion concentration ($HCO_3^-$), carbonate ($CO_3^{2-}$), carbon dioxide ($CO_2$) concentrations, partial pressure of carbon dioxide ($pCO_2$), calcite saturation index ($\Omega_{Cal}$) and aragonite saturation index ($\Omega_{Ara}$) were determined by total alkalinity (TA), pH, temperature, pressure, and salinity using the QuickBASIC program CO2sys software (Pierrot et al., 2006) with the set of constants (Mehrbach, 1973) and refit by Dickson and Millero (1987), and $KHSO_4$ according to Dickson (1990). Dissolved inorganic carbon (DIC) was estimated by the sum of the $HCO_3^-$, $CO_3^{2-}$, and $CO_2$. TA was determined during all the three stages:

177 acclimatization period (days 3 and 8), the $CO_2$ exposure to reach pH 7 (days 17, 22, 28, 32, 36, 45,
178 52, and 60), and the recovery period (days 66, 70 and 74). Water samples were collected in
179 triplicate in the input and output of the Titank. The pH was measured with electrode sonde (pH
180 meter, model MeterLab). Seawater was titrated with hydrochloric acid (HCl 0.02 M) to reach two
181 different pH values (3.8 and 3.6) of the equivalence point. Accuracy of the method was verified by
182 random samples of seawater fixed with HgCl and analyzed by the Norwegian Institute for Water
183 Research (NIVA, Oslo-Norway).
184
185 *2.3.3. Element analysis in sediment*
186 Dried sediment was acid digested following the Community Bureau of Reference BCR- sequential
187 extraction (F1: acid soluble- acetic acid, F2: easily reducible- hydroxylamine hydrochloride, F3:
188 oxidizable- hydrogen peroxide and ammonium acetate) (Rauret et al., 1999). The sum of the
189 fractions (F1+F2+F3) is considered as the mobile phase (Pérez-López et al., 2009). Dissolved
190 element concentrations (As, Ca, Cd, Cu, Fe, Mg, Na, Ni, P, Pb, and Zn) in extracts were analysed
191 by means of High-Resolution Inductive Coupled Plasma Mass Spectrometry (HR-ICP-MS Element
192 2, Thermo-Finnigan). The BCR-701 reference material standard was used for sediment-extractable
193 certification. The agreement of the analysis results and certified values were above 90%.

194 *2.3.4. Element bioaccumulation in soft tissue*

195 For the assessment of elements bioaccumulated in soft tissue, individual freeze-dried samples (30.8
196 ± 18.8 mg dw) were processed by microwave digestion using a Milestone Ultra Clave (UC). Each
197 sample was placed into a Teflon tube (PFA, 18 mL) with 2 mL 50% v/v ultra-pure $HNO_3$ (distilled
198 using Milestone SubPur). The pressure was set to 160 bar and the temperature was gradually
199 increased to 245 °C for 1 hour and 15 minutes followed by a cooling period of 1 hour. After
200 digestion, the samples were diluted in Milli-Q water (18.2 MΩ/cm) to a final volume of 16.8 ± 0.9
201 mL to achieve a concentration of 0.6 M $HNO_3$. The concentration of elements was determined

using High-Resolution Inductive Coupled Plasma Mass Spectrometry HR-ICP-MSwith PFA-Schott type spray chamber and nebulizer. The samples were introduced using an SC2 DX autosampler and a prepFAST auto dilution system. The certified reference material used in the trace metal recovery and the analytical method for the biological tissue: the certified Oriental Basma Tobacco Leaves (INCT OBTL-5) and dogfish muscle (DORM-3) from NRC (Detection limits can be found in supplementary material Table S1)

The uptake rate (*Ku*- uptake concentration per unit of time) was calculated as detailed in Kalman et al. (2015). The bioaccumulation factor (*BAF*) was determined as the relationship between the concentrations in the organism and concentrations in the bioavailable form in the environment (Drexler et al., 2003).

*2.3.5. Statistical approach*

Data of element concentration in the soft tissue of clams were checked for normality and homogeneity with Levene´s tests. Significant differences ($\alpha = 0.05$) between initial element concentration in the soft tissue of clams, exposed clams (into the TiTank: pre-injection, pH 6,9 phase, and recovery, see Figure 2d), and external experiment groups were determined using a one-way ANOVA followed by the Bonferroni multiple post hoc comparison using Statgraphics Statistical Programme. Linear regression of element concentrations on soft tissue against time was calculated with the PRISM 5.0 Statistical Software. An analysis of the variance (ANOVA) followed by a Tukey post hoc test was carried out to determine differences in the Ca/Mg ratios in soft tissue of the clams.

## 3. Results

225 3.1. Carbonate system speciation

226 Changes in the seawater carbonate system parameters during the experimental period are
227 summarised in Table 1. During the period without $CO_2$ injection, water chemistry remained
228 constant. However, when $CO_2$ was injected the increase in $pCO_2$ promoted a decrease in the
229 carbonate system with lowered pH, and thus saturation indexes also decreased. Once the $CO_2$
230 injection was stopped the carbonate system recovered gradually to reach the initial conditions after
231 14 days.

**Table 1.** Bicarbonate ($HCO_3^-$), carbonate ($CO_3^{2-}$), carbon dioxide ($CO_2$), dissolved inorganic carbon (DIC), calcite saturation index ($\Omega_{Cal}$), aragonite saturation index ($\Omega_{Ara}$) and partial pressure of carbon dioxide ($pCO_2$) were determined as part of the **c**arbonate system speciation in seawater using the CO2SYS program. Carbon parameters were calculated based on total pH (±0.05), temperature (8±0.2), pressure (29 bars) and salinity (31±0.5) from outflow seawater samples ($n$ = 3).

| Day | Treatment | TA | | $HCO_3$ | | $CO_3^{2-}$ | | $CO_2$ | | DIC | | $\Omega_{Cal}$ | | $\Omega_{Ara}$ | | $pCO_2$ | |
|---|---|---|---|---|---|---|---|---|---|---|---|---|---|---|---|---|---|
| | (pH) | µmol kgSW$^{-1}$ | | µmol kgSW$^{-1}$ | | µmol kgSW$^{-1}$ | | µmol kgSW$^{-1}$ | | µmol kgSW$^{-1}$ | | | | | | bar | |
| | | *av* | *sd* | *av* | *sd* | *av* | *sd* | *av* | *sd* | *av* | *sd* | *av* | *sd* | *av* | *sd* | *av* | *sd* |
| 3 | Acclimatization (7.9) | 2286 | 31.3 | 2091 | 28.5 | 78.7 | 1.38 | 31.1 | 0.33 | 2201 | 30.2 | 1.808 | 0.032 | 1.144 | 0.020 | 674 | 7.23 |
| 8 | Acclimatization (7.9) | 2282 | 28.6 | 2040 | 25.4 | 97.9 | 1.57 | 23.6 | 0.23 | 2162 | 27.2 | 2.251 | 0.036 | 1.423 | 0.023 | 509 | 5.00 |
| 17 | $CO_2$ injection (7.1) | 2247 | 35.3 | 2215 | 34.8 | 12.76 | 0.26 | 213 | 2.61 | 2441 | 37.7 | 0.293 | 0.006 | 0.185 | 0.004 | 4561 | 56.4 |
| 22 | $CO_2$ injection (6.9) | 2257 | 19.3 | 2239 | 19.1 | 7.42 | 0.08 | 375 | 2.49 | 2621 | 21.7 | 0.170 | 0.002 | 0.107 | 0.001 | 8009 | 53.9 |
| 28 | $CO_2$ injection (6.9) | 2246 | 49.0 | 2229 | 48.6 | 6.69 | 0.19 | 409 | 6.93 | 2645 | 55.7 | 0.154 | 0.004 | 0.097 | 0.003 | 8715 | 149 |
| 32 | $CO_2$ injection (6.9) | 2235 | 42.8 | 2216 | 42.4 | 7.61 | 0.19 | 354 | 5.27 | 2578 | 47.9 | 0.175 | 0.004 | 0.110 | 0.003 | 7551 | 114 |
| 36 | $CO_2$ injection (6.9) | 2208 | 33.6 | 2192 | 33.4 | 6.48 | 0.13 | 403 | 4.76 | 2602 | 38.3 | 0.150 | 0.003 | 0.094 | 0.002 | 8582 | 102 |
| 45 | $CO_2$ injection (6.9) | 2244 | 38.6 | 2230 | 38.3 | 5.81 | 0.13 | 466 | 6.22 | 2702 | 44.7 | 0.134 | 0.003 | 0.084 | 0.002 | 9908 | 134 |
| 52 | $CO_2$ injection (6.9) | 2258 | 13.2 | 2240 | 13.1 | 7.04 | 0.05 | 387 | 1.76 | 2635 | 14.9 | 0.162 | 0.001 | 0.102 | 0.001 | 8231 | 37.8 |
| 60 | $CO_2$ injection (6.9) | 2247 | 19.1 | 2225 | 18.9 | 8.59 | 0.09 | 314 | 2.07 | 2548 | 21.1 | 0.198 | 0.002 | 0.125 | 0.001 | 6699 | 44.6 |
| 66 | Recovery (7.5) | 2241 | 13.8 | 2170 | 13.3 | 28.8 | 0.23 | 87.5 | 0.42 | 2286 | 14.0 | 0.667 | 0.005 | 0.419 | 0.003 | 1828 | 8.83 |
| 70 | Recovery (7.9) | 2295 | 34.4 | 2100 | 31.4 | 79.2 | 1.53 | 30.2 | 0.35 | 2210 | 33.3 | 1.835 | 0.035 | 1.154 | 0.022 | 637 | 7.46 |
| 74 | Recovery (7.9) | 2281 | 32.05202 | 2102 | 29.4 | 72.4 | 1.31 | 33.2 | 0.36 | 2208 | 31.1 | 1.676 | 0.030 | 1.055 | 0.019 | 704 | 7.73 |

239 3.2. Element concentration in sediments

240 The median element concentrations (As, Ca, Cd, Cu, Fe, Mg, Na, Ni, P, Pb, and Zn) sediment
241 samples are presented in Table 2. In general, the concentration in the bioavailable form did not vary
242 appreciably during exposure and recovery. However, there was a decreasing trend of Ca from 5515
243 µg $g^{-1}$ at the beginning of the experiment to 4711 µg $g^{-1}$ at the end, and a sharp increase in Na
244 concentration (from 12.9 to 14.5 mg $g^{-1}$). Also, Pb and Zn displayed an increase of bioavailable
245 concentration in the in sediments. Further sediment characterization of Trondheim Fjord sediments
246 is detailed in Basallote et al. (2020).

247

248 **Table 2.** Median element concentration in sediments ($n$ = 3) from Trondheim Fjord collected after
249 the different stages in the TiTank according to the experimental set up (Figure 2d).

| | | *Acclimatization* | *Injection $CO_2$* | | | *Recovery* |
|---|---|---|---|---|---|---|
| *Days* | | 14 | 10 | 25 | 39 | 14 |
| *As* | µg $g^{-1}$ | 3.91 | 3.35 | 4.04 | 5.43 | 3.48 |
| *Ca* | µg $g^{-1}$ | 5515 | 5448 | 5130 | 5179 | 4911 |
| *Cd* | µg $g^{-1}$ | 0.02 | 0.02 | 0.02 | 0.02 | 0.02 |
| *Cu* | µg $g^{-1}$ | 18.6 | 17.7 | 18.2 | 18.6 | 18.5 |
| *Fe* | mg $g^{-1}$ | 8.57 | 8.58 | 8.49 | 9.40 | 8.63 |
| *Mg* | µg $g^{-1}$ | 4471 | 4361 | 4528 | 4595 | 4574 |
| *Na* | mg $g^{-1}$ | 12.9 | 12.6 | 13.5 | 13.3 | 14.5 |
| *Ni* | µg $g^{-1}$ | 14.4 | 14.2 | 14.4 | 15.6 | 15.0 |
| *P* | µg $g^{-1}$ | 540 | 509 | 559 | 579 | 545 |
| *Pb* | µg $g^{-1}$ | 17.7 | 18.0 | 18.1 | 20.5 | 19.3 |
| *Zn* | µg $g^{-1}$ | 59.1 | 58.6 | 59.7 | 65.1 | 61.5 |

250

251 3.3. Biological responses

252 *3.3.1. Lethality, outer shell deterioration, and shell growth rates*

253

No significant lethality occurred in exposed or external group. Two out of 132 clams died ($n_{TiTank}$ = 60; $n_{external}$ = 60; $n_{background}$ = 12). Distinct calcein marking and were missing from 15.3% of clams and these were omitted from the growth analyses (Supplementary material Figure S2.1). Significant variability in growth was observed between individuals and almost half of the marked clams (48,5%) had no detectable shell growth (Figure S2.1). For individuals with detectable growth no significant differences were observed in shell growth between clams exposed to $CO_2$ (pH 6.9) at 29 atm and the external group at 1 atm and pH 7.97 (Figure 4, $p$ = 0.59). From the growth rate data (µm x day$^{-1}$; supplementary material Figure S2.2 and S2.3) it was apparent that the individuals that had no detectable growth were in the larger size class ($p$ < 0.0001). The total size range was 8 to 21.5 mm and 91% (43 individuals) of the clams that did not display shell growth had a shell length above 15 mm. Furthermore, there were no difference in size distribution of the growing individuals between the exposed and control group ($p$ = 0.60). The same applied to the size distribution between exposed and non-exposed for individuals not growing ($p$ > 0.90; supplementary material Figure S2.3).

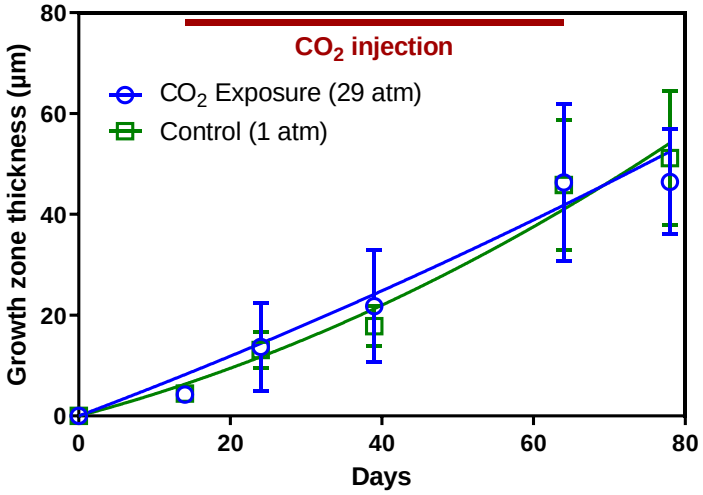


**Figure 4. Mean** shell growth zone in clams from Titank (29 atm, blue) and external clam group (1 atm, green). Curves were created by second-order polynomial fit. Clams with no shell growth were

omitted. Vertical bars indicate standard error ($n$ = 5-7, except for day 14 where $n_{TiTank}$ = 2 and $n_{external}$ = 3, total $n_{TiTank}$ = 23 and $n_{external}$ = 27).

### *3.3.2. Bioaccumulation in soft tissue*

Elements analysed in the soft tissue of clams exposed to $CO_2$ were statistically compared with background concentrations and external experiment population (Figure 5). Some of the elements such as As, Cu, Ni or Fe showed a decrease of element concentration in tissue over time. However, for Cd, Cr, Pb, and Ti, no significant differences ($p > 0.05$) were found between exposed clams, the corresponding external group and the background level. Other elements, such as As, Cu, Ni, and Fe displayed significant differences ($p < 0.05$) between groups (Figure 5a) but also a reduction in metal(loid) concentration in tissue over time independent of exposure to $CO_2$ and pressure (Figure 5b). However, the slopes of the decline in concentrations between exposed and the external groups of clams were not significantly different for As, Cu, and Fe. In contrast, the corresponding slopes for Ni tissue concentrations were significantly different.

Calcium uptake was nearly constant in clams from the external group (-1.55 ± 3.9 µg $g^{-1}$ dw $d^{-1}$), but strongly ($p < 0.05$) declined in concentration in tissue in TiTank clams (-18.9 ± 3.1 µg $g^{-1}$ dw $d^{-1}$). A similar trend was observed for P, with significant differences ($p < 0.05$) between the exposed and non-exposed group with -31.1 ± 4.5 and -8.5 ± 3.9 µg P $g^{-1}$dw $d^{-1}$, respectively. Contrary, Na and Mg were significantly bioaccumulated in soft tissue during the course of the experiment in both groups, reaching values of *Ku* during $CO_2$ injection of 111 ± 103 and 9.97 ± 9.1 µg $g^{-1}$ dw $d^{-1}$, respectively (Figure 6).

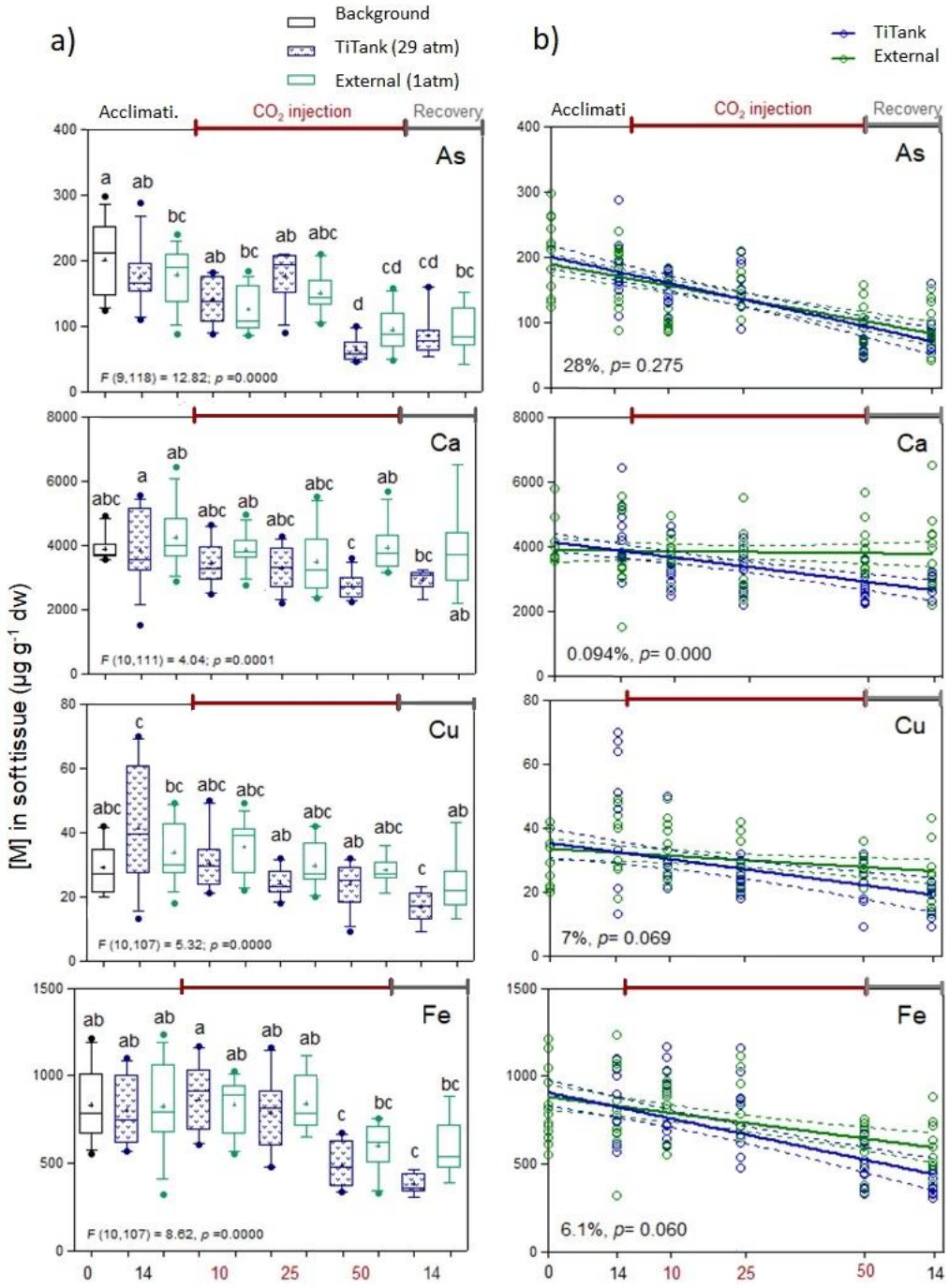
a)
b)
Background
TiTank (29 atm)
External (1atm)
TiTank
External
Acclimati.
Acclimati
CO2 injection
Recovery
As
Ca
Cu
Fe
[M] in soft tissue (µg g-1 dw)
F (9,118) = 12.82; p =0.0000
F (10,111) = 4.04; p =0.0001
F (10,107) = 5.32; p =0.0000
F (10,107) = 8.62, p =0.0000
28%, p= 0.275
0.094%, p= 0.000
7%, p= 0.069
6.1%, p= 0.060
0
14
10
25
50
14

292

293

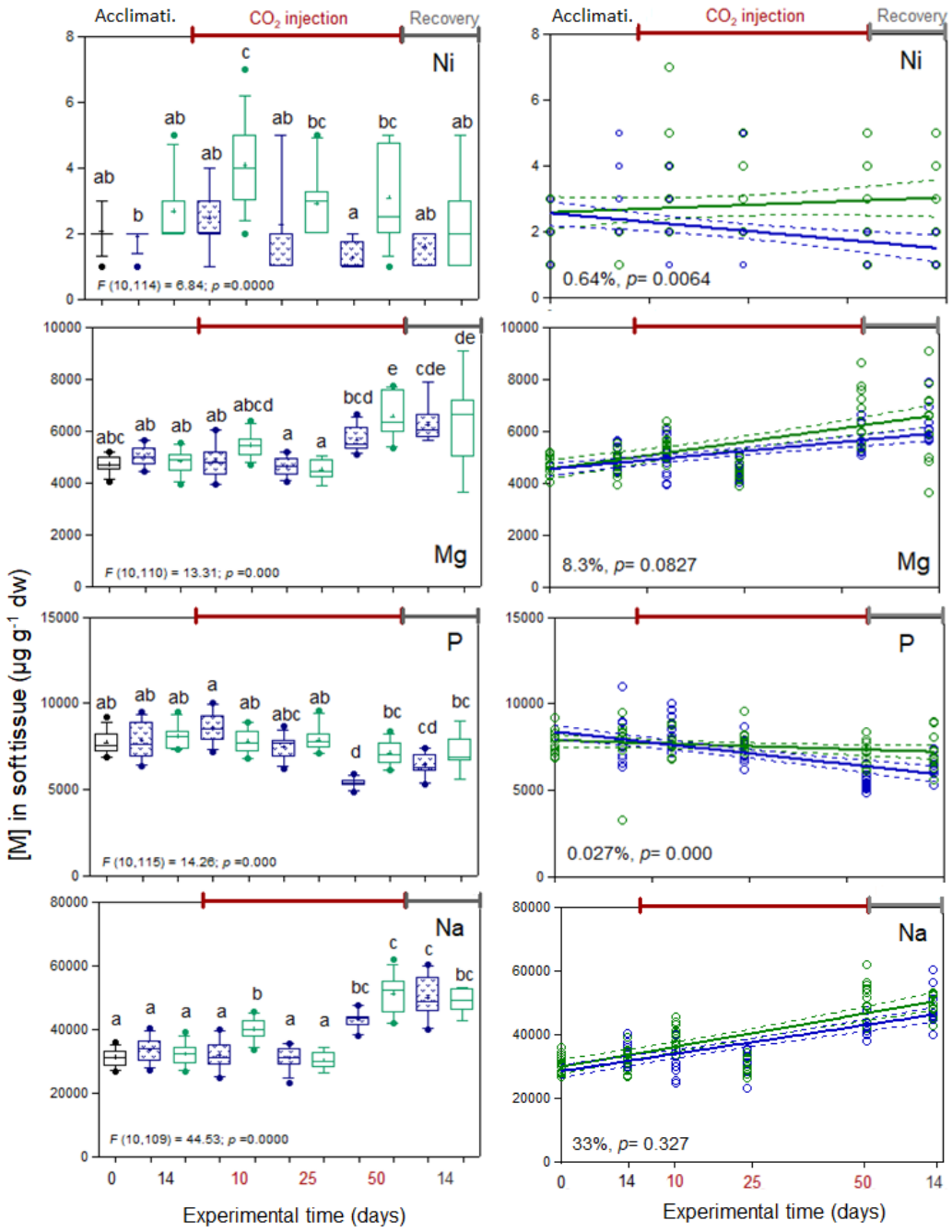


**Figure 5.** a) Metal(loid) concentration in the soft tissue of clams *Astarte* sp. (µg $g^{-1}$ dw) exposed in the TiTank (blue), the external experiment (green) and the background concentration (black) along the experimental timeline (pre-$CO_2$ injection-14 days; $CO_2$ exposure - 50 days; $CO_2$ cessation or recovery- 14 days). Different letters above the boxplots are indicating significant differences ($p < 0.05$) as noted by the ANOVA. b) Linear regression of element bioaccumulation in the soft tissue of exposed clams (blue) and external group (green) along the timeline (days).

301

302 *3.3.3. Bioaccumulation factors and uptake rates*

303 In general, during acclimatization, there was an increasing tendency of *BAF*; however, after $CO_2$
304 injection, different *BAF* patterns were observed showing a negative tendency of the
305 bioaccumulation in tissue (As, Ca, Cd, Cu, Fe, Ni, P, Pb, and Zn), except for Na and Mg. After $CO_2$
306 injection was stopped, a trend of stabilizing *BAF* values for most of the studied elements, except for
307 (Fe, Cu, Na, and Mg) was observed.

308 The *Ku* values did not follow any particular pattern. Just in the acclimatization period *Ku* values
309 were positive for most of the studied elements (except As and P). Then, there was a downward
310 trend in uptake rates. The negative value of *Ku* implies a decrease of the element concentration
311 from tissue, i.e., the biological responses for the negative tendency of *Ku* would be indicating i)
312 elimination (*Ke*) of elements from soft tissue or abiotic transfer (adsorption of metal outside of soft
313 cell), or ii) increase of soft tissue weight (growth dilution). This first statement is difficult to
314 confirm without other biological modeling parameters. While the second statement was already
315 confirmed by the observed shell growth during the experimental period (Figure 4). On the other
316 hand, the concentration in the environment in the bioavailable form (Table 2) was stable during the
317 experiment (except for Na). This supports growth dilution as the reason for negative *Ku* and *BAF*
318 trends during the $CO_2$ exposure period.

319

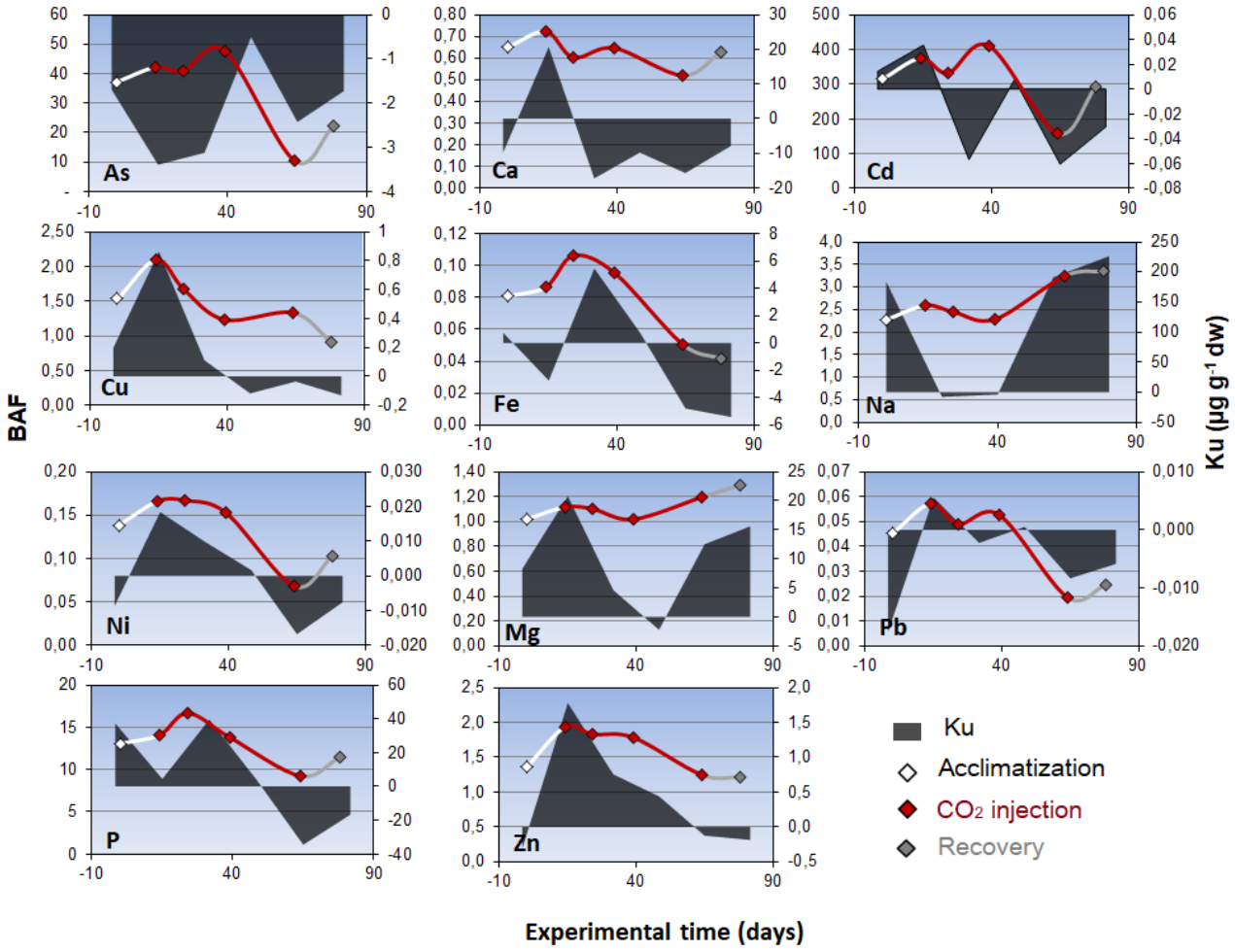


320

321 **Figure 6.** Bioaccumulation factor (*BAF*) and uptake rates (*Ku*) evolution for the TiTank
322 experiment.

323 Figure 7 plots the ratio Mg/Ca evolution in soft tissue of Astarte in the experimental conditions.
324 This ratio remained below 2 without $CO_2$ injection, but increased with when acidification started. It
325 reached a significant value after 50 day of exposure conditions, and a slight decline after $CO_2$
326 injection cessation.

327 After acidification, the ratios in the recovery period showed no significant ($p > 0.05$) differences,
328 with an increment of the double *Ku* of Ca (-15.7 (d 50- exposure) to -7.86 (d 14- recovery) µg Ca $g^{-1}$
329 dw).

330

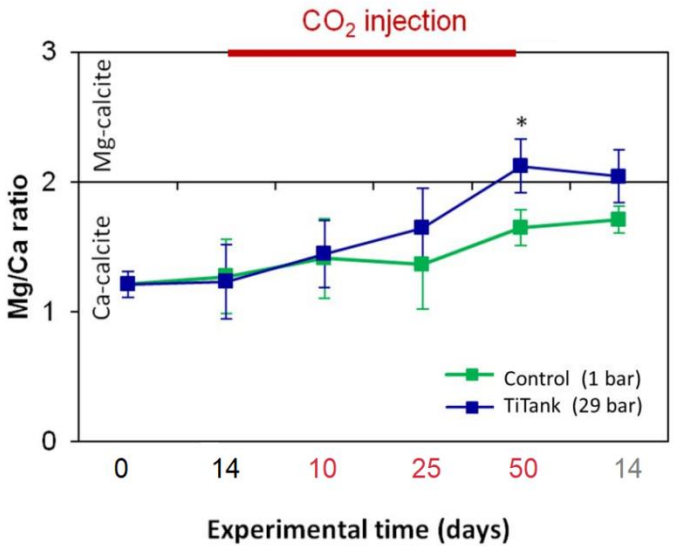


331

332 **Figure 7**. Evolution of the ratio Mg/Ca in soft tissue of the clam during exposures associated with
333 the Titank (Experimental) and the external group (green). Asterisk denotes the significant
334 differences of the ANOVA followed by a Tukey post hoc test ($p < 0.05$).

335

336 4. Discussion

337 Leakages from the sub-seabed $CO_2$ storages can promote environmental changes provoking
338 responses in the biota (Sokołowski et al., 2018; Świeżak et al., 2018; Molari et al., 2019). Assessing
339 the risks associated with these leakages requires consideration of: (i) physical/chemical
340 environment- the magnitude of the leakage and the impact over the environment; i.e., how much the
341 environment is modified, and if the environment can recover back to the initial state once the stress
342 has ceased; and, (ii) biological impact- responses of the different organisms (as species) to the
343 stressor; i.e., how vulnerable they are to the new state of the physical/chemical environment and
344 assess if reversible or irreversible biological effects has occurred.

345 The pH is controlled by the buffer capacity of the seawater through a chemical equilibrium between
346 carbonate species (Dickson and Millero, 1987). When there is an excess of $CO_2$, this equilibrium is

modified, affecting the carbon speciation as it is observed in Table 1. While total alkalinity (TA) remained stable, all the remaining carbon system parameters changed significantly when $CO_2$ is injected. However, when the $CO_2$ injection stopped, the equilibrium returned the initial status, i.e., results showed the replacement of the water and washout of acid water promotes the carbon system returns to its initial and typical values (Table 1). The observed shift in the saturation indexes would be affecting the speciation of elements, which might trigger the mobilization of elements into the environment and, consequently, toxic responses exhibited by the affected organisms. In this case, the biological responses reflecting changes were analysed as lethal (mortality) and sub-lethal (shell-growth rate, and bioaccumulation) endpoints (Figures 4, 5, and 6).

The most evident response of organisms against an extreme environmental stress is lethality. No lethal effect was recorded during the experimental environmental modifications of conditions. Therefore, no lethal risk was associated with reducing the pH from about 8 to 6.9 for *Astarte* sp. For 7 weeks. This is in accordance with previous studies reported in Gazeau et al. (2013) that confirm no likely lethality on molluscs over exposure times ranging from 8 to 30 days. In contrast, juvenile stages of the clam *Ruditapes philippinarum* showed around a 5 % increase of mortality after 10 days of exposure to pH 6.9 (Basallote et al., 2015). Similar rates (> 95 % survival) were recorded under the same conditions for adult stages of *R. philippinarum* (Rodríguez-Romero et al., 2014b). The higher mortality for clams reported by Rodriguez-Romero et al. (2014b) may be explained by pollution of the sediments from Huelva, which is an area subjected to high metal content coming from mining activities and chemical industries. The combination of high metal concentration in sediments together with $CO_2$ seems to be more critical than $CO_2$-derived acidification itself in adult clams. However, some other studies found negative effects in the early stages of clams (Świeżak et al., 2018) and sea-urchin (Basallote et al., 2018) at pH 6.9 with metallic sediment, which determined higher vulnerability of early stages of those species for low pH. Metal mobilization promoted by acidification (Ardelan and Steinnes, 2010; DeOrte et al., 2014; Basallote

et al., 2020) may cause lethality. However, low bioavailable concentrations of elements released from the Trondheim Fjord sediments in the case of a $CO_2$ leakage promoting acidification to pH 6.9 (Table 2) are below the lethal threshold for *Astarte* sp. (111-232 mm shell length).

An increasing trend of the bioavailable form of Fe and Pb in the sediments with acidification at pH 6,9 was observed (Table 2). A similar trend was observed by Basallote et al. (2020) who determined the element distribution of Trondheim Fjord sediments using diffusive gradient thin films (DGT) samplers and concluded that acidification increased the dissolved concentration of Fe (in $Fe^{2+}$ form in the water column) Ce and Pb. In accordance with their research, Cd was not affected by the simulated leakage in our experiment. The concentration pattern of Fe and Pb in the acidified water was not reflected in the tissue of the clams (Figure 5).

There were differences in background concentrations over time. It seemed holding time had a larger effect on more trace elements than pressure/acidification. So, that, bioaccumulation was not observed by *Astarte* sp. for most of the studied elements (Figure 5) despite De Orte et al. (2014) reported mobilization of metal(loid)s from sediment to water column. Also, a previous study with sediments from Gdansk Bay showed considerable mobilization at pH 7.0, although not as much as at pH 6.3 (personal communication, Murat V. Ardelan, 2019). In this sense, mobilization may not only be a function of pH, but may be influenced by the type, and the geochemical composition of the sediment. Therefore, a range of gradients of pH and sediment types are essential to determine risk assessment (DelValls et al., 2019).

Ocean acidification leads to substantial impacts on marine organisms, especially to calcifiers, due to carbonate ion (aragonite) concentration saturation being reduced. The TiTank treatments led to calcite and aragonite undersaturation ($\Omega_{Cal} < 1$; $\Omega_{Ara} < 1$, Table 1). Although corals are the target species as the most sensitive calcifiers to ocean acidification (DeCarlo et al., 2018), bivalves might be also affected by the same micro-scale internal calcifying space. Several authors (Gazeau et al.,

2013; Clements and Hunt, 2017) have stated that the most sensitive process to decreasing pH appears to be shell dissolution that might occur upon exposure to pH values slightly below 7.5 for some bivalves, such as *Pinctata fucata* (Kawatani and Nishii, 1969) or *Venesuosis decusata* (Bamber, 1987). Besides, early developmental stages are particularly sensitive to pH changes, such as mollusk larvae of the *Haliotis tubertulata* (Wessel et al., 2018), which increased the malformation and unshelled larvae when reducing pH from 8.0 to 7.7 and 7.6, referent values for ocean acidification; notwithstanding $CO_2$ leakage with corresponding values below pH 7.0. In this sense, malformations in the early stages of *Limecola balthica* were observed at pH 7.0 and 6.3 (1 atm) (Świeżak et al., 2018). Despite the effort for cleaning outside shell in the current study, this technique for image assessment to determine the damage of acidification to external calcification was discarded for initial damages and loss of calcein adhesion. However, the fluorochrome stain allowed measuring the shell growth rate. The peripheral part of the shell is composed of anterior, ventral and posterior areas and has active bio-mineralization (Linard et al., 2011). Positive growth of the Baltic bivalve *Limecola balthica* exposed to a pH 7.0 (under atmospheric pressure) confirmed high biomineralization rates as an adaptation to natural increments in $CO_2$ (Sokołowski et al., 2018). Results of the shell growth rate in *Astarte* sp. (Figure 4) confirmed that the thickness of the shell of some individuals increased up to 50 µm in the experimental time (79 days) independently of environmental changes related to acidification. However, only about half of the marked clams did grow and 15% of the total population of 130 was not stained during the marking procedure. Clams of the genus Astarte are slowing growing and highly tolerant to anaerobiosis (Oeschger, 1990). It is therefore not unlikely that some of the clams remained closed during the time submerged in the Calcein solution avoiding their mantle fluid to be exposed. The observed growth rates were highly variable and clearly related to size and presumably age of the clams with lager clams dominating the non-growing fraction. This may be related to both a generally lower growth rate in lager clams but also to season (autumn) and that mature clams are prioritizing allocating

421 energy to reproductive tissue. A potentially suboptimal food source (live algae) may also influence
422 growth. However, when compared to the control group kept in natural seawater (pH 7.96, 1 atm)
423 shell growth pattern and survival did not seem to be affected by pressure (29 atm) and 7 weeks of
424 $CO_2$ exposure with associated drop to pH 6.9.

425 Previous studies in bivalves have observed that carbonate mineral saturation state determines the
426 settler's responses (Green et al., 2013). Conditions in the TiTank simulated a marine system where
427 carbonate saturation state is normally under-saturated for calcium carbonate (considering constant
428 P, T, and S, pH~7; Table 1). Therefore, the main source of Ca for shell growth (reflected by natural
429 growth, Figure 4) was incorporated through metabolism (Figure 5). This might be the immediate
430 step before incorporation into the shell. However, Andersson et al. (2008) determined that marine
431 calcifiers from cold water (high latitudes) generate hard parts rich in Mg-calcite deposits as
432 response to immediate risk to ocean acidification (decrease of seawater carbonate saturation).

433 Only Mg and Na concentration in soft tissue increased significantly over the exposure time (Figure
434 5). Magnesium is linked to energy availability (growth), temperature, and seawater carbonate
435 saturation state (Moberly, 1968). Surprisingly, Mg uptake has been demonstrated to be negative in
436 low pH conditions for corals (Ries, 2011); in contrast to bivalves in the current experiment, which
437 registered a significant increase of Mg concentration in tissue in detriment of Ca for exposed clams
438 (Figure 5). When pH values decrease there is a decrease in the saturation of Ca-calcite and
439 aragonite precipitates (Lippmann, 1973); so that, for bivalves surrounded by seawater with high Mg
440 concentration, there is a displacement of Ca from calcite by Mg. At the low temperature of the
441 experiment (8°C), it might favor the formation of a metastable phase, where Ca ions start to be
442 replaced by smaller Mg ions in the carbonate calcite promoting dolomite and isomorphs of calcite
443 (Chave, 1952). According to Checa et al. (2006), the deposition of high-Mg calcite is located in the
444 margins of the shell (Figure 3 and 4). However, incorporation of Mg-calcite in shell growth needs
445 further research. In the biomineralization process of the shells, the ratio of Mg/Ca in the soft tissue

446 of the bivalves is loosely linked with carbon chemistry in the deep seabed, being conditioned by the
447 availability of elements according to carbonates speciation (Table 1). After exposure to carbon
448 dioxide leakages under pressure and low temperature, the ratio Mg/Ca is inverted to values above 2
449 (Figure 7). This might be pointing to an uptake of $Mg^{2+}$ for incorporation in the shell at high
450 pressure, mirroring the geological processes. In contrast, without pressure, $Ca^{2+}$ incorporation is
451 preponderant for aragonite and calcium calcite shell formation.

452

453 5. Conclusions

454 Moderate leakages of carbon dioxide from sub-seabed in the Norwegian shelf deposits might cause
455 toxic effects and/or physiological damages in bivalves, but the magnitude of the effects is
456 proportional to the acidification promoted in the environment. The target bivalve used, *Astarte* sp.,
457 did not display lethal responses or significant bioaccumulation of toxic elements in soft tissue. This
458 lowered pH (6.9) did not affect the growth rates of the clams. An increase of Mg in detriment of Ca
459 in the soft tissue of clams may be a first early warning response of this slight acidification as a
460 result of altered geological equilibrium and seawater saturation.

461 Although significant research has been performed to assess risks associated with $CO_2$ leakages,
462 there are not enough findings to demonstrate effects over a wide range of taxa or varied life
463 strategies. Filling the knowledge gaps of potential exposure, risks, and damage derived from
464 leakages of $CO_2$ from potential CCS sites is important for reliable environmental risk assessment.
465 Further research with more extreme conditions (greater acidification and contaminated sediments,
466 and more species and life stages) would be necessary to understand chemical and biological
467 mechanisms of responses.

468

469 Credit Author Statement

470 **Estefanía Bonnail**: Methodology, Validation, Formal analysis, Investigation, Data curation,
471 Writing- Original draft preparation, Writing - Review & Editing, Visualization**. Ana R. Borrero-**
472 **Santiago**: Methodology, Validation, Formal analysis, Investigation, Data curation, Writing -
473 Original Draft, Writing-Review & Editing, Visualization. **Trond Nordtug**: Methodology, Formal
474 analysis, Investigation, Writing - Review & Editing, Visualization, Supervision, Project
475 administration. **Ida Beathe Øverjordet**: Methodology, Formal analysis, Investigation, Writing -
476 Review & Editing, Visualization. **Daniel Franklin Krause**: Methodology, Software, Validation,
477 Investigation, Writing - Review & Editing, Visualization. **Murat V. Ardelan**: Conceptualization,
478 Methodology, Validation, Formal Analysis, Resources, Writing - Review & Editing, Supervision,
479 Project administration, Funding acquisition.

480

481 Acknowledgments

482 The authors thank the Research Council of Norway for the financial support by CLIMIT program
483 (Trykk$CO_2$ Project: Environmental impacts of leakage from sub-seabed $CO_2$ storage, grant
484 254777/E20). E Bonnail thanks ANID/FONDECYT (Folio N°11180015).

485

486 References

487 Abele-Oeschger, D., Oeschger R., 1995. Hypoxia-induced autoxidation of haemoglobin in the
488 benthic invertebrates *Arenicola marina* (Polychaeta) and *Astarte borealis* (Bivalvia) and the
489 possible effects of sulphide. J. Exp. Mar. Biol. Ecol., https://doi.org/10.1016/0022-
490 0981(94)00172-A

491 Andersson, A.J., Mackenzie, F.T., Bates, N.R., 2008. Life on the margin: implications of ocean
492 acidification on Mg-calcite, high latitude and cold-water marine calcifiers. Mar. Ecol.
493 Progress Series, https://doi.org/10.3354/meps07639

494 Ardelan, M.V., Steinnes, E., 2010. Changes in mobility and solubility of the redox sensitive metals
495 Fe, Mn and Co at the seawater-sediment interface following $CO_2$ seepage. Biogeosciences,
496 7(2), 569-583. https://doi.org/10.5194/bg-7-569-2010

497 Ardelan, M.V., Steinnes, E., Lierhagen, S. et al., 2009. Effects of experimental $CO_2$ leakage on
498 solubility and transport of seven trace metals in seawater and sediment. Sci. Total Environ.,
499 https://doi.org/10.1016/j.scitotenv.2009.09.004

500 Ardelan, M.V., Sundeng, K., Slinde, G.A., et al., 2012. Impacts of possible $CO_2$ seepage from sub-
501 seabed storage on trace elements mobility and bacterial distribution at sediment-water
502 interface. Energy Procedia, http://dx.doi.org/10.1016/j.egypro.2012.06.047

503 Bachu, S., Adams, J.J., 2003. Sequestration of $CO_2$ in geological media in response to climate
504 change: capacity of deep saline aquifers to sequester $CO_2$ in solution. Energy Convers.
505 Manag., https://doi.org/10.1016/S0196-8904(03)00101-8

506 Bamber, R.N., 1987. The effects of acidic sea water on young carpet shell clams *Venerupsis*
507 *desussata*, L., Mollusca: Veneracea. J. Exp. Mar. Biol. Ecol., 108, 241–260.

508 Basallote, M.D., Rodríguez-Romero, A., De Orte, M.R., et al., 2015. Evaluation of the threat of
509 marine $CO_2$ leakage-associated acidification on the toxicity of sediment metals to juvenile
510 bivalves. Aquat. Toxicol., https://doi.org/10.1016/j.aquatox.2015.07.004

511 Basallote, M.D., Rodríguez-Romero, A., De Orte, M.R., DelValls, T.Á., Riba, I., 2018.
512 $CO_2$ leakage simulation: effects of the pH decrease on fertilisation and larval development of
513 *Paracentrotus lividus* and sediment metals toxicity. Chem. Ecolog.,

514 https://doi.org/10.1080/02757540.2017.1396319

515 Basallote, M.D., Borrero-Santiago, A.R., Cánovas, C.R., Hammer, K.M., Olsen, A.J., Ardelan,
516 M.V., 2020. Trace metal mobility in sub-seabed sediments by $CO_2$ seepage under high-
517 pressure conditions. Sci. Total Environ., https://doi.org/10.1016/j.scitotenv.2019.134761

518 Bautista-Chamizo, E., De Orte, M.R., DelValls, T.A., Riba, I., 2016. Simulating $CO_2$ leakages from
519 CCS to determine Zn toxicity using the marine microalgae *Pleurochrysis roscoffensis*.
520 Chemosphere, https://doi.org/10.1016/j.chemosphere.2015.09.041

521 Borrero-Santiago, A.R., Carbú, M., DelValls, T.A., Riba, I., 2016. $CO_2$ leaking from sub-seabed
522 storage: Responses of two marine bacteria strains. Mar. Environ. Res.,
523 https://doi.org/10.1016/j.marenvres.2016.05.018

524 Borrero-Santiago, A.R., DelValls, T.A., Riba, I., 2017. Bacterial community responses during a
525 possible $CO_2$ leaking from sub-seabed storage in marine polluted sediments. Sci. Total
526 Environ., https://doi.org/10.1016/j.scitotenv.2017.03.153

527 Borrero-Santiago, A.R., Ribicic, D., Bonnail, E., Netzer, R., Koseto, D., Ardelan, M.V., 2020.
528 Response of bacterial communities in Barents Sea sediments in case of a potential
529 CO2 leakage from carbon reservoirs. Mar. Environ. Res.,
530 https://doi.org/10.1016/j.marenvres.2020.105050

531 Checa, A.G., Jiménez-López, C., Rodríguez-Navarro, A., Machado, J.P., 2006. Precipitation of
532 aragonite by calcitic bivalves in Mg-enriched marine waters. Mar. Biol.,
533 https://doi.org/10.1007/s00227-006-0411-4

534 Chave, K.E., 1952. A solid solution between calcite and dolomite. J Geol 60:190–192.

535 Clements, J.C., Hunt, H.L., 2017. Effects of $CO_2$-driven sediment acidification on infaunal marine

536 bivalves: A synthesis. Mar. Pollut. Bull., https://doi.org/10.1016/j.marpolbul.2017.01.053

537 Conradi, M., Sánchez-Moyano, J.E., Galotti, A., et al., 2019. $CO_2$ leakage simulation: Effects of the
538 decreasing pH to the survival and reproduction of two crustacean species. Mar. Pollut. Bull.,
539 https://doi.org/10.1016/j.marpolbul.2019.04.020

540 DeCarlo, T.M., Comeau, S., Cornwall, C.E., McCulloch, M.T., 2018. Coral resistance to ocean
541 acidification linked to increased calcium at the site of calcification. Proc. R. Soc. B,
542 http://doi.org/10.1098/rspb.2018.0564

543 DelValls, A., Souza, L.S., Aloise, A., Pereira, C.D.S., et al., 2019. Integrative assessment of
544 sediment quality in acidification scenarios associated with carbon capture and storage
545 operations. Environ. Rev., https://doi.org/10.1139/er-2018-0084

546 De Orte, M.R., Lombardi, A.T., Sarmiento, A.M., Basallote, M.D., Rodriguez-Romero, A., Riba, I.,
547 Del Valls, A., 2014. Metal mobility and toxicity to microalgae associated with acidification of
548 sediments: $CO_2$ and acid comparison. Mar. Environ. Res.,
549 https://doi.org/10.1016/j.marenvres.2013.10.003

550 De Orte, M.R., Bonnail, E., Sarmiento, A.M., et al., 2018. Metal fractionation in marine sediments
551 acidified by enrichment of $CO_2$: A risk assessment. Mar. Pollut. Bull.,
552 https://doi.org/10.1016/j.marpolbul.2018.04.072

553 Dewar, M., Wie, W., McNeil, D., Chen, B., 2013. Small-scale modelling of the physiochemical
554 impacts of $CO_2$ leaked from sub-seabed reservoirs or pipelines within the North Sea and
555 surrounding waters. Mar. Pollut. Bull., https://doi.org/10.1016/j.marpolbul.2013.03.005

556 Dickson, A.G., Millero, F.J., 1987. A comparison of the equilibrium constants for the dissociation
557 of carbonic acid in seawater media. Deep Sea Res. Part A Oceanogr Res. Pap.,
558 https://doi.org/10.1016/0198-0149(87)90021-5

559 Dickson, A.G., 1990. Standard potential of the reaction: AgCl(s) + 1/2 $H_2$(g) = Ag(s) + HCl(aq),
560 and the standard acidity constant of the ion $HSO_4^-$ in synthetic sea water from 273.15 to
561 318.15 K. J Chemosphere Thermodyn 22, 113−127. https://doi.org/10.1016/0021-
562 9614(90)90074-Z

563 Drexler, J., Fischer, N., Henningsen, G., et al., 2003. Issue paper on the bioavailability and
564 bioaccumulation of metals. U.S. Environmental Protection Agency. Risk Assessment
565 Forum. Retreived from archives of the USEPA.
566 https://archive.epa.gov/raf/web/pdf/bioavail_bioaccum_aug03.pdf

567 Gazeau, F., Parker, L.M., Comeau, S., et al., 2013. Impacts of ocean acidification on marine shelled
568 mollusks. Mar. Biol., https://doi.org/10.1007/s00227-013-2219-3

569 Geological Survey of Norway, Marine maps, 2017. Norges Geologiske Undersøkelse Marine Kart,
570 2017.
571 http://geo.ngu.no/kart/marin/MARINEKART.html?kart=5&latlon=63.5,10.5&zoom=10#

572 Global C.C.S. Institute., 2017. Global Costs of Carbon Capture and Storage - 2017 Update 14.

573 Green, M.A., Waldbusser, G.G., Hubacz, L., Cathcart, E., Hall, J., 2013. Carbonate mineral
574 saturation state as the recruitment cue for settling bivalves in marine muds. Estuaries Coasts,
575 https://doi.org/10.1007/s12237-012-9549-0

576 IPCC, 2013. Working Group I Contribution to the IPCC Fifth Assessment Report, Climate Change
577 2013: The Physical Science Basis. IPCC AR5, 2014.

578 Kalman, J., Bonnail-Miguel, E., Smith, B.D., Bury, N.R., Rainbow, P.S., 2015. Toxicity and the
579 fractional distribution of trace metals accumulated from contaminated sediments by the clam
580 *Scrobicularia plana* exposed in the laboratory and the field. Sci. Total Environ.,
581 https://doi.org/10.1016/j.scitotenv.2014.11.013

582 Kawatani, Y., Nishii, T., 1969. Effects of pH of culture water on the growth of the Japanese pearl
583 oyster. Bull. Jpn. Soc. Fish Sci. 35, 342–350.

584 Leung, D.Y.C., Caramanna, G., Maroto-Valer, M.M., 2014. An overview of current status of
585 carbon dioxide capture and storage technologies. Renew. Sust. Energ. Rev.,
586 https://doi.org/10.1016/j.rser.2014.07.093

587 Lichtschlag, A., James, R.H., Stahl, H., Connelly, D., 2015. Effect of a controlled sub-seabed
588 release of $CO_2$ on the biogeochemistry of shallow marine sediments their pore waters and
589 the overlying water column. Int. J. Green. Gas Control,
590 https://doi.org/10.1016/j.ijggc.2014.10.008

591 Linard, C., Gueguen, Y., Moriceau, J., et al., 2011. Calcein staining of calcified structures in pearl
592 oyster *Pictada margaritifera* and the effect of food resource level on shell growth.
593 Aquaculture, https://doi.org/10.1016/j.aquaculture.2011.01.008

594 Lippmann, F., 1973. *Sedimentary carbonate minerals*. Springer, Berlin

595 Market Reports World, 2019. Global carbon capture and storage (CCS) market- Segmented by
596 technology end-user industry and geography-growth, trends and forecasts, 2018-2023. INH-
597 12344751. 5 april 2018. pp.146.

598 Market Research Report (MMR), 2016. Carbon Capture and Storage (CCS) Market Size & Forecast
599 Report, 2014 - 2025. Report ID: MN 17612895. Grand View Research, pp. 104

600 Mehrbach, C., 1973. Measurement of the Apparent Dissociation Constants of Carbonic Acid in
601 Seawater at Atmospheric Pressure.

602 Moberly R., 1968. Composition of magnesian calcites of algae and pelecypods by electron
603 microprobe analysis. Sedimentology, 11, 61–82.

Molari, M., Guilin, K., Lott, C., Weber, M., de Berr, D., Meyer, S., et al., 2018. $CO_2$ leakage alters biogeochemical and ecological functions of submarine sands. Sci. Advances, https://doi.org/10.1126/sciadv.aao2040

Molari, M., Guilini, K., Lins, L., Ramette, A., Vanreusel, A., 2019. $CO_2$ leakage can cause loss of benthic biodiversity in submarine sands. Sci. Total Environ., https://doi.org/10.1016/j.marenvres.2019.01.006

NDP, 2010. http://www.npd.no/Global/Engelsk/3%20-%20Publications/Reports/OneNorthSea/OneNortSea_Final.pdf

Oeschger, R. (1990). "Long-term anaerobiosis in sublittoral marine invertebrates from the Western Baltic Sea: Halicryptus spinulosus (Priapulida), Astarte borealis and Arctica islandica (Bivalvia)." Marine Ecology Progress Series 59: https://doi.org/10.3354/meps059133

Olsen, B.R., Grahl-Nielsen, O., Schander, C., 2009. Population study of *Astarte sulcata*, da Costa, 1778, (Mollusca, Bivalvia) from two Norwegian fjords based on the fatty acid composition of the adductor muscle. Biochem. System. Ecol., https://doi.org/10.1016/j.bse.2009.10.003

Payán, M.C., Verbinnen, B., Galan, B., et al., 2012. Potential influence of $CO_2$ release from a carbon capture storage site on release of trace metals from marine sediment. Environ. Pollut., https://doi.org/10.1016/j.envpol.2011.10.015

Pérez-López, R., Séz, R., Álvarez-Valero, A.M., Nieto, J.M., Pace, G., 2009. Combination of sequential chemical extraction and modelling of dam-break wave propagation to aid assessment of risk related to the possible collapse of a roasted sulphide tailings dam. Sci. Total Environ., https://doi.org/10.1016/j.scitotenv.2009.07.031

Pierrot, D.E., Lewis, A., Wallace, D.W.R., 2006. MS Excel program developed for center, $CO_2$ system calculations. In: ORNL/CDIAC-105a. Carbon Dioxide Information Analysis Oak

627 Ridge National Laboratory. U.S. Department of Energy, Oak Ridge, Tennessee.
628 https://doi.org/10.3334/CDIAC/otg.CO2SYS_XLS_CDIAC105

629 Rauret, G., López-Sánchez, J.F., Sahuquillo, A., et al., 1999. Improvement of the BCR three step
630 sequential extraction procedure prior to the certification of new sediment and soil reference
631 materials. J. Environ. Monitor., 1, 57-61.

632 Ries, J.B., 2011. Skeletal mineralogy in a high $CO_2$ world. J. Exp. Mar. Biol. Ecol.,
633 https://doi.org/10.1016/j.jembe.2011.04.006

634 Riis, F., Halland, E., 2014. $CO_2$ storage atlas of the Norwegian Continental shelf: Methods used to
635 evaluate capacity and maturity of the $CO_2$ storage potential. Energy Procedia,
636 https://doi.org/10.1016/j.egypro.2014.11.557

637 Rodríguez-Romero, A., Basallote, M.D., De Orte, M.R., et al., 2014a. Simulation of $CO_2$ leakages
638 during injection and storage in sub-seabed geological formations: Metal mobilization and
639 biota effects. Environ. Intern., https://doi.org/10.1016/j.envint.2014.03.008

640 Rodríguez-Romero, A., Jiménez-Tenorio, N., Basallote, M.D., et al., 2014b. Predicting the impacts
641 of $CO_2$ leakage from subseabed storage: Effects of metal accumulation and toxicity on the
642 model benthic organism *Ruditapes philippinarum.* Environ. Sci, Technol.,
643 https://doi.org/10.1021/es501939c

644 Sneli, J.A., 1998. A simple benthic sledge for shallow and deep-sea sampling. Sarsia,
645 https://doi.org/10.1080/00364827.1998.10413670

646 Sokołowski, A., Brulińska, D., Mirny, Z., et al., 2018. Differing responses of the estuarine bivalve
647 *Limecola balthica* to lowered water pH caused by potential $CO_2$ leaks from a sub-seabed
648 storage site in the Baltic Sea: An experimental study. Mar. Pollut. Bull.,
649 https://doi.org/10.1016/j.marpolbul.2017.09.037

650 Świeżak, J., Borrero-Santiago, A.R., Sokołowski, A., Olsen, A.J., 2018. Impact of environmental
651 hypercapnia on fertilization success rate and the early embryonic development of the clam
652 *Limecola balthica*., Bivalvia, Tellinidae) from the southern Baltic Sea - A potential
653 $CO_2$ leakage case study. Mar. Pollut. Bull., http://doi.org/10.1016/j.marpolbul.2018.09.007

654 Theede, H., Ponat, A., Hiroki, K., Schlieper, C., 1969. Studies on the resistance of marine bottom
655 invertebrates to oxygen-deficiency and hydrogen sulphide. Mar. Biol., 2: 325-337.

656 Vilarrasa, V., Bolster, D., Dentz, M., et al., 2009. Effects of $CO_2$ compressibility on $CO_2$ storage in
657 deep saline aquifers. Transp. Porous. Med., http://dx.doi.org/10.1007/s11242-010-9582-z

658 Wessel, N., Martin, S., Badou, A., et al., 2018. Effect of $CO_2$–induced ocean acidification on the
659 early development and shell mineralization of the European abalone (*Haliotis tuberculata*).
660 J. Exp. Mar. Biol. Ecol., https://doi.org/10.1016/j.jembe.2018.08.005

661 Zetter, M.L. 2001. Recent geographical distribution of *Astarte borealis* species complex, its
662 nomenclature and bibliography. Schr. Malakozoo. 18:1-14. ISSN 0936-2959.